

Dualism of the $4f$ electrons and high-temperature antiferromagnetism of the heavy-fermion compound YbCoC_2

D. A. Salamatin^{1,2}, N. Martin³, V. A. Sidorov¹,
N. M. Chtchelkatchev^{1,4}, M. V. Magnitskaya^{1,5},
A. E. Petrova^{1,5}, I. P. Zibrov¹, L. N. Fomicheva¹, Jing Guo⁶,
Cheng Huang⁶, Liling Sun⁶, and A. V. Tsvyashchenko¹

¹Institute for High Pressure Physics, Russian Academy of Sciences, 14 Kaluzhskoe shosse, 108840 Troitsk, Russia

²Joint Institute for Nuclear Research, 141980 Dubna, Moscow Region, Russia

³Université Paris-Saclay, CNRS, CEA, Laboratoire Léon Brillouin, 91191 Gif-sur-Yvette, France

⁴Ural Federal University, 19 Mira str., 620002 Ekaterinburg, Russia

⁵P.N. Lebedev Physical Institute of the Russian Academy of Sciences, 53 Leninskiy prospekt, 119991 Moscow, Russia

⁶Institute of Physics, Chinese Academy of Sciences, 100190 Beijing, P. R. China

Abstract

We report on the first study of the noncentrosymmetric ternary carbide YbCoC_2 . Our magnetization, specific heat, resistivity and neutron diffraction measurements consistently show that the system behaves as a heavy-fermion compound, displaying an amplitude-modulated

magnetic structure below the Néel temperature reaching $T_N = 33$ K under pressure. Such a large value, being the highest among the Yb-based systems, is explained in the light of our *ab initio* calculations, which show that the $4f$ electronic states of Yb have a dual nature – i.e., due to their strong hybridization with the $3d$ states of Co, $4f$ states expose both localized and itinerant properties.

The dual nature of the $5f$ and $4f$ -electrons, i.e. the coexistence of localized and itinerant states in a variety of actinide and rare-earth (RE) heavy-fermion systems (e.g., UPt₃, UPd₂Al₃ Takahashi et al. [1996], UGe₂ Troć et al. [2012], Yaouanc et al. [2002], Haslbeck et al. [2019], PuCoGa₅ Booth et al. [2012], YbRh₂Si₂ Danzenbächer et al. [2011], YbAl₃ Ebihara et al. [2000]) is the subject of an intense discussion. A theory for the electronic excitations in uranium compounds, based on the localization of two $5f$ electrons, was developed by Zwicknagl and Fulde Zwicknagl and Fulde [2003]. The standard model for $4f$ -electrons in RE metals and their compounds is that an integral number of $4f$ electrons are assumed being localized at each RE ion site. This applies to both “normal” REs, where a single $4f$ configuration of given occupation is stable, and to mixed-valent cases, where fluctuations between states with different integral $4f$ occupations take place. The nature of magnetism (itinerant or localized) and the competition between ordered and disordered ground states in these mixed-valent (“abnormal”) RE elements (Ce, Eu and Yb), remain a major challenge in condensed matter physics. In this context, the Kondo effect and the Ruderman–Kittel–Kasuya–Yosida (RKKY) interaction arising between itinerant and localized $4f$ -electrons play essential roles, as originally pointed out by Doniach Doniach [1977].

The noncentrosymmetric carbide YbCoC₂, first synthesized more than 30 years ago Jeitschko and Gerss [1986], represents an interesting platform for studying such physics. Here, we report on *the first study* of its bulk magnetic and transport properties at ambient and elevated pressure, complemented by neutron diffraction measurements and *ab initio* calculations. We show that YbCoC₂ is a heavy-fermion compound with an amplitude modulated incommensurate magnetic order. Its Néel temperature is the highest among Yb³⁺-based systems, exceeding the previous record value belonging to β -YbAlB₄ Tomita et al. [2016]. Taken together, our experimental and numerical results indicate that the dual nature of the $4f$ electrons is essential for understanding the magnetic and transport properties of YbCoC₂.

The transition from localized to itinerant electron states signalling the onset of large-range electronic correlations, is also of great interest. In lanthanides this effect is related to Ce, the first element with a single $4f$ electron level. The Yb intermetallic compounds are usually considered as being dominated by two valence states, where Yb^{3+} ions can be seen as f -hole analogs of Ce. Owing to such an electronic configuration, one can anticipate a dual character of $4f$ states in YbCoC_2 , with transitions from localized states to itinerant ones. Heavy-fermion magnetism in Yb-based systems with localized $4f$ electrons mainly occurs in compounds where the ordering temperatures is low (typically, $T_N < 10$ K), for instance in YbNi_2 Rojas et al. [2012], YbNiSn Kasaya et al. [1992], YbPtGe Katoh et al. [2009], Tsujii et al. [2015], YbPdGe Tsujii et al. [2015], Enoki et al. [2012] or YbRh_2Si_2 Gegenwart et al. [2002], YbPtBi Fisk et al. [1991], Ueland et al. [2014]. In fact, many such compounds displaying antiferromagnetic (AFM) order, T_N is even below 1 K (e.g., YbIr_2 Willis et al. [1985], YbPd Pott et al. [1985], YbX ($X = \text{N, P, As}$) Ott et al. [1985] and YbXCu_2 ($X = \text{Au, Pd}$) Rossel et al. [1987]). [Few exceptions are YbBe_{13} ($T_N = 1.3$ K) Walter et al. [1985], Yb_3Pd_4 ($T_N = 3$ K) Pollit et al. [1985] and YbB_2 ($T_N = 5.7$ K) Avila et al. [2003].] At atmospheric pressure, the highest magnetic transition temperature is $T_N = 20$ K observed recently in $\alpha\text{-YbAl}_{1-x}\text{Mn}_x\text{B}_4$ for $x = 0.27$ Suzuki et al. [2018]. The pressure-induced magnetic ordering was found in the heavy-fermion superconductor $\beta\text{-YbAlB}_4$ Tomita et al. [2015], where the magnetic transition temperature increases up to 32 K, obtained under the external pressure P of 8 GPa Tomita et al. [2016].

Previously it has been established that the magnetic structure of the $R\text{CoC}_2$ compounds (where R is a heavy RE element), isostructural to YbCoC_2 , is ferromagnetic (FM). The magnetic moments usually point along the a axis Schfer et al. [1997], except in DyCoC_2 where they lie in the ac plane Amanai et al. [1995]. The magnetic susceptibility measurements in YCoC_2 and the refinements of neutron powder diffraction patterns of other $R\text{CoC}_2$ compounds indicate that the Co and C ions are non-magnetic Schfer et al. [1990], Amanai et al. [1995]. Notably, the Curie temperature for $R\text{CoC}_2$ compounds deviates from the de Gennes law De Gennes, P.G. [1962], Schfer et al. [1997], indicating the importance of the interactions beyond RKKY in the stabilization of the magnetic order in this series and calls for further studies of the nature of magnetism in these systems.

Polycrystalline samples of YbCoC_2 were synthesized by melting Yb, Co and C (see Ref. Tsvyashchenko [1984]) at 8 GPa and 1500-1700 K using

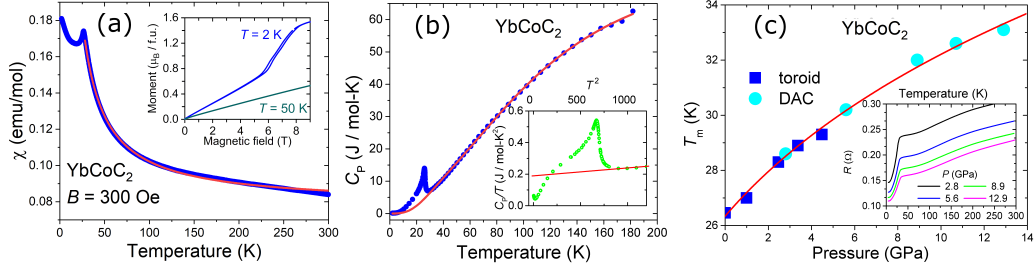


Figure 1: (a) Temperature-dependence of the magnetic susceptibility χ of YbCoC₂, measured in the external magnetic field $B=300$ Oe (blue points). The red line is the fit of a modified Curie-Weiss law to the $T=28$ –300 K data (see the text for details). Inset: isothermal magnetization of YbCoC₂ measured in the $B = 0$ –9 T field range at $T = 2$ and 50 K. (b) Temperature-dependence of the heat capacity C_p of YbCoC₂ (blue points). The red line is the fit of two Debye laws to the high-temperature data, extrapolated down to $T \rightarrow 0$ (see the text). Inset: the low-temperature part of C_p/T vs. T^2 . The red line is the linear approximation of C_p/T vs. T^2 extended down to 0 K. (c) Pressure-dependence of the magnetic transition temperature T_m measured in the toroid and diamond-anvil (DAC) high-pressure cells (blue squares and light blue circles, respectively). The red line is the approximation with the function $f(P - P_{c0})^\alpha$, where $f = 18.6$ K/GPa^{1/5}, $P_{c0} = -5.7$ GPa and $\alpha = 1/5$. Inset: temperature-dependence of the isobaric electrical resistance, measured at $P = 2.8$ –12.9 GPa.

Toroid high-pressure cell. The Rietveld analysis of x-ray and neutron diffraction data at $T = 300$ K shows that the compound crystallizes in an orthorhombic structure of the CeNiC₂-type (space group $Amm2$, no. 38), similar to other RE carbides $RCoC_2$. High-pressure X-ray diffraction measurements performed at the 15U beamline of the Shanghai Synchrotron Radiation Facility (China) show that the orthorhombic crystal structure is preserved up to 37 GPa sup. A fit of a Murnaghan equation of state volume vs. pressure data yields a bulk modulus $B_0 = 176(23)$ GPa, with its first pressure derivative $B'_0 = 9(1)$. The bulk magnetic properties of YbCoC₂ were studied by vibrating sample magnetometry (VSM) using a physical property measurement system (PPMS). The electrical resistivity measurements were performed on bulk polycrystalline samples using a lock-in detection technique Petrova et al. [2005]. The high-pressure resistance measurements

below 5 GPa were performed in a miniature clamped Toroid-type device with glycerine–water (3:2) liquid as the pressure transmitting medium. For higher pressures a diamond-anvil cell (DAC) with NaCl as the pressure transmitting medium was used.

The magnetic susceptibility $\chi(T)$ measured in the magnetic field $B = 300$ Oe exhibits a sharp peak, indicative of an AFM-like transition at $T_N = 25.6(2)$ K (Fig. 1a). In the $T = 28$ –300 K-range, $\chi(T)$ can be well-described by a modified Curie–Weiss law $\chi = \chi_0^* + C^*/(T - \theta)$, where χ_0^* is a temperature-independent term, C^* - the Curie constant and θ - the Weiss constant. The effective magnetic moment deduced from this approximation is $\mu_{\text{eff}} = 4.31(1) \mu_B$ per formula unit (f.u.), a value close to that of the free Yb^{3+} ion ($4.54 \mu_B$). The small positive Weiss constant $\theta = 2.4(1)$ K reveals the presence of weak ferromagnetic correlations and a small value of the ratio $f_s = \theta/T_N \approx 0.09 \ll 1$ indicates a weak level of spin frustration in the system.

The inset of Fig. 1a shows field-dependences of the bulk magnetization M measured in the $B = 0$ –9 T-range at $T = 2$ and 50 K. At $T = 50$ K, $M(H)$ has a smooth linear character, typical of a paramagnet. In contrast, the curve measured at $T = 2$ K $< T_N$ first increases linearly up to ≈ 6 T, until a field-induced ferromagnetic transition with a hysteresis of about 0.2 T takes place in the ≈ 6 –8 T-range. M does not fully saturate at the highest field of 9 T and reaches a value of $\approx 1.6 \mu_B/\text{f.u.}$, which stands well-below the theoretical saturation moment for the full Yb^{3+} multiplet ($\mu_s = 4.0 \mu_B$).

Fig. 1b displays the temperature-dependence of the heat capacity C_P , obtained in the 2-180 K range. Around T_N , the $C_P(T)$ curve exhibits a lambda anomaly, with a maximum at ≈ 26 K, which is consistent with the bulk AFM-like transition deduced from the $\chi(T)$ data. The heat capacity jump at T_N is equal to $\Delta C_P(T_N) = 14.64$ J/mol-K. This value is close to the one calculated for an amplitude modulated magnetic structure for Yb^{3+} , namely 13.43 J/mol-K Blanco et al. [1991]. The heat capacity at $T > 30$ K was approximated by $C_{\text{fit}}(T) = m_1 D(T, \Theta_1) + m_2 D(T, \Theta_2)$, where D is the Debye function, with the characteristic temperatures $\Theta_1 = 516(11)$ K and $\Theta_2 = 176(7)$ K. The best fit was obtained with the coefficients $m_1 = 2.49(4)$ and $m_2 = 0.79(5)$. The magnetic entropy of the transition computed according to $S_m(T) = \int_{1.9 \text{ K}}^T C_m(T)/T dT$, where $C_m(T) = C_P(T) - C_{\text{fit}}(T)$ is the magnetic part of heat capacity, amounts to 3.91 J/mol-K at $T = 30$ K. This value is about 70 % of that expected for a magnetic doublet ground state and

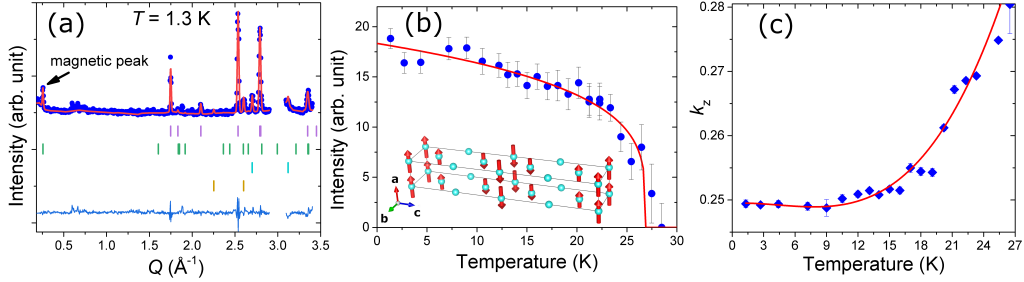


Figure 2: (a) Refined neutron powder-diffraction pattern of YbCoC_2 measured at $T = 1.3$ K and ambient pressure: the experimental points (blue dots), the calculated profiles (red line) and their difference (light blue line). The bars in the lower part of the graph represent the calculated Bragg reflections that correspond to the nuclear $Amm2$ structure (first row, purple), the magnetic phase (second row, green), the aluminum container (third row, cyan), and the non-magnetic impurity phase YbO (fourth row, brown). (b) Temperature-dependence of the square-root of the integrated intensity of the magnetic peak (blue circles). The red line is the power law fit (see the text). Inset: Schematic representation of the magnetic unit cell of YbCoC_2 in the commensurate phase (only Yb magnetic atoms are shown). (c) Temperature-dependence of the k_z component of the magnetic wave vector (blue diamonds). The red line is drawn to guide the eye.

is most likely due to Kondo screening Blanco et al. [1994]. The Sommerfeld coefficient obtained from the C_P data just above T_N , is $\gamma = 190(1)$ mJ/mol-K² (see inset of Fig. 1b). This value suggests a considerable enhancement of the effective electron mass in YbCoC_2 comparable with other heavy-fermion compounds Katano et al. [2017], Motoya et al. [1997]. The low temperature upturn in C_P/T (see the inset of Fig 1b) indicates that there is a possibility of the second magnetic transition in YbCoC_2 similar to the incommensurate-commensurate magnetic transition in CeNiC_2 Motoya et al. [1997].

As shown in Fig. 1c, the electrical resistance increases monotonically with temperature revealing the metallic character of YbCoC_2 . Because of the coherent scattering of charge carriers in the magnetically ordered state, the resistance drops down below the AFM-like transition temperature (see inset of Fig. 1c). Interestingly, the transition temperature T_m , determined from the onset of the resistance, increases with external pressure up to 33.2(3) K at $P = 13$ GPa.

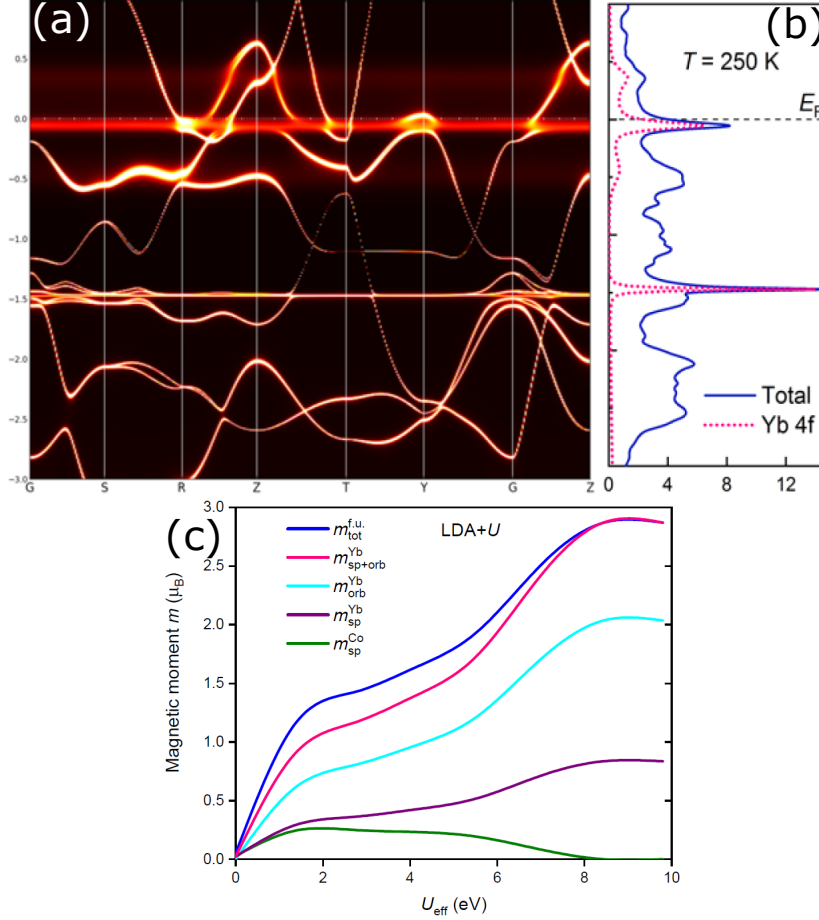


Figure 3: The DMFT band structure (a) and DOS (b) at $T = 250$ K. The DOS is in arb. units and the Fermi energy is set to zero. (c) The LDA+ U calculations: the magnetic moment per formula unit and its partial contributions as functions of U_{eff} . The green line is the spin moment of Co, the violet line is the spin moment of Yb, the cyan line is the orbital moment of Yb, the red line is the total moment of Yb and the blue line is the total magnetic moment.

In order to elucidate the magnetic structure of YbCoC_2 , we have used neutron powder diffraction (NPD) on the thermal instrument G4-1 (Laboratoire Léon Brillouin). The low temperature patterns display an additional peak at low angles (see Fig. 2a). The square-root of the integrated intensity

of this peak depends on temperature (see Fig. 2b) and may be approximated with the function $\sigma_0(1 - T/T_C)^\beta$, with the critical exponent $\beta = 0.24(4)$ and the critical temperature $T_C = 26.9(7)$ K. This peak can be indexed with the wave vector $(0, 0, k_z)$, where k_z is temperature-dependent (see Fig. 2c). The best refinement of the magnetic part of neutron powder diffraction pattern is achieved by assuming an amplitude modulated (sine-wave) structure of Yb³⁺ magnetic moments, pointing along the a axis with the amplitude $1.32(7) \mu_B$ at $T = 1.3$ K. Such a value of magnetic moment is typical for Yb in magnetic compounds Tsujii et al. [2015], Chattopadhyay et al. [2018], Yaouanc et al. [2016], Ueland et al. [2014] and may be attributed to the crystal electric field effects and a partial screening due to the Kondo mechanism. The structure locks into a commensurate state with $k_z = 1/4$ at $T_{\text{lock-in}} \approx 8$ K.

The *ab initio* simulations of YbCoC₂ were performed using the Wien2k package Blaha et al. [2018] within the density functional theory (DFT) and the local density approximation (LDA), with the spin-orbit coupling (SOC) taken into account. The $4f$ electrons of the Yb ion were explicitly treated as valent and not completely localized, and as such were allowed to and hybridize with all other states. The calculations started from the experimental lattice parameters measured in this work, with subsequent relaxation of internal atomic coordinates. In these initial DFT-LDA calculations ($T = 0$ K), a nonmagnetic (paramagnetic) ground state of YbCoC₂ was determined, whereas no magnetic solution turned out to be stable.

From the band structure and density of states (DOS) of paramagnetic YbCoC₂ it follows sup that $4f$ states of Yb are present at the Fermi energy (E_F), and the main contribution to the total DOS at E_F stems from the strongly hybridized ytterbium f - and cobalt d -states. The energy bands in the vicinity of E_F are flat, which indicates a strong enhancement of the electron mass to a value typical for heavy-fermion systems.

To treat strong electron correlations in the Yb $4f$ shell adequately, we further employed the combination of DFT-LDA Blaha et al. [2018] and dynamical mean field theory (DMFT) Kotliar et al. [2006] as implemented in the eDMFT package Haule et al. [2010]. Since the DMFT method is not applicable to the low-temperature region, for simulations of the magnetic state of YbCoC₂ observed experimentally below 30 K we have used the LDA+ U approach Anisimov et al. [1993], Liechtenstein et al. [1995] in the Wien2k implementation, which can perform zero-temperature calculations with accounting for correlation effects of $4f$ electrons.

The band structure and DOS computed at $T = 250$ K using DMFT are

shown in FIG. 3(a, b). The evaluated number of $4f$ electrons is about 13.05, i.e. the valence of Yb is actually equal to three. There is a certain similarity between the DFT and DMFT results in the number of $4f$ electrons and in the position of the bands and corresponding DOS peaks sup. Within both approaches, the Fermi energy falls into a steep slope of the $4f$ DOS whose maximum is very close to E_F . Apparently, the proximity of $4f$ peak to E_F and the resulting relatively high $N(E_F)$, as well as a significant f - d hybridization favour the high magnetic transition temperature for YbCoC₂.

In our LDA+ U simulations of the magnetic state only the $4f$ electron correlations were taken into account. The positions of the bands are found to shift downwards with increasing $U_{\text{eff}} = U - J$ (where U and J are the standard on-site Coulomb interaction constants). We obtained a stable FM ordering with the periodicity of the crystal lattice. The total magnetic moment and its main partial atomic contributions as functions of U_{eff} are depicted in Fig. 3(c). The largest partial contribution (including both the spin and orbital terms) is μ_{Yb} directed along the a axis in accordance with the experimental data and drawn in Fig. 3(c) as the red line. This is the magnetic moment of the Yb site which increases with U_{eff} . The magnetic moment of Co is smaller tending to zero with increasing U_{eff} , whereas the magnetic moments at carbon sites and in the interstitial region are negligible at any U_{eff} .

The interval of U_{eff} between 1.3 and 3.5 eV has been considered as optimal, corresponding to the experimental situation. The change in U_{eff} in this interval does not lead to a strong variation of the magnetic moments and band positions. The Yb moment varies from 0.9 to 1.3 μ_B , which correlates well with the experimental observations. The model of ferromagnetic alignment used in the calculations turned out to be quite reasonable, because the period of experimental modulated magnetic structure is about four times that of the crystal lattice. Moreover the Yb magnetic moments are co-directed to each other within the crystallographic unit cell (see the inset in Fig. 2b). Thus, our LDA+ U calculations demonstrate that YbCoC₂ possesses a stable magnetic ordering with the magnetization predominantly located at the Yb sites.

A wealth of experimental and numerical results presented in this study, unambiguously establishes that the noncentrosymmetric YbCoC₂ is an unusual heavy-fermion system, displaying incommensurate antiferromagnetic ordering with the transition temperature reaching 33 K under pressure. The nature of its magnetic structure is surprising in itself, since the isostructural compounds $RCoC_2$ (where $R = \text{Gd-Tm}$) display FM ordering. This fact is

well captured by our *ab initio* calculations, which also reproduce the direction of the Yb magnetic moments and, quantitatively, their amplitude. As a key result, we reveal a strong hybridization between the $4f$ states of Yb and the $3d$ orbitals of Co. We believe that this feature is instrumental in explaining the robustness of the magnetic order and its enhancement under applied external pressure. Another appealing finding concerns the evolution of the magnetic structure with pressure. Indeed, a fine-tuning of the tight competition between RKKY and Kondo interactions is a well-proven route towards the observation of quantum criticality, exotic forms of superconductivity and novel strange metallic states.

Acknowledgement

This work was supported by Russian Science Foundation: D.A.S., V.A.S., A.E.P., and A.V.T. acknowledge the support of their experimental work (grant by the RSF No. 17-12-01050); N.M.C. and M.V.M. are grateful for support of their theoretical calculations (Grant RSF 18-12-00438). The results of calculations were obtained using computational resources of MCC NRC ‘Kurchatov Institute’ (<http://computing.nrcki.ru/>) and supercomputers at Joint Supercomputer Center of RAS (JSCC RAS). We also thank the Uran supercomputer of IMM UB RAS for access.

Supplementary Information

Abstract

We present supplementary information on the details of experimental techniques and *ab initio* calculations discussed in the main text.

Experimental techniques

The purity of constituent elements of YbCoC_2 were 99.7% for Yb, 99.9% for Co and 99.99% for C. For high-pressure x-ray diffraction measurements at the 15U beamline of the Shanghai Synchrotron Radiation Facility a monochromatic x-ray beam with a wavelength of 0.6199 Å was employed and silicon oil was used as a pressure-transmitting medium. The pressure for all measurements in the DACs was determined by the ruby fluorescence method Mao et al. [1986].

X-ray powder diffraction measurements at room temperature and ambient pressure were performed using the diffractometer Guinier camera G670, Huber (Cu- $K\alpha_1$). This XRD pattern was analyzed with GSAS software Larson and Dreele [2000]. NPD patterns were analyzed with the Rietveld and Le Bail methods using FULLPROF software Rodriguez-Carvajal [1993]. The measured lattice constants are in agreement with previous determinations Jeitschko and Gerss [1986].

Structure

The unit cell of this structure is shown in together with its first Brillouin zone (right). Planes of Yb ions perpendicular to the a direction alternate with the planes of Co and C ions shifted along the a direction by $a/2$ (see FIG. S4). The C ions exist as dimers with the C-C nearest distance of 1.55 Å, double bonds between them shown with green sticks. Red sticks indicate the nearest distance between two Yb ions equal to the a lattice period (3.44 Å), which hardly assumes essential direct exchange between localized $4f$ electrons of Yb. The impurity of high-pressure phase of non-magnetic ytterbium oxied (YbO) with a fraction of less than 5% wt. was also found in the samples.

X-ray diffraction patterns of YbCoC_2 obtained at different pressures are presented in FIG. S5. The dependencies of the lattice constants and unit

cell volume of YbCoC_2 under high pressure up to 37 GPa are presented in FIG. S6.

The results of Rietveld refinements of XRD and NPD patterns at room temperature and atmospheric pressure are presented in Table 1.

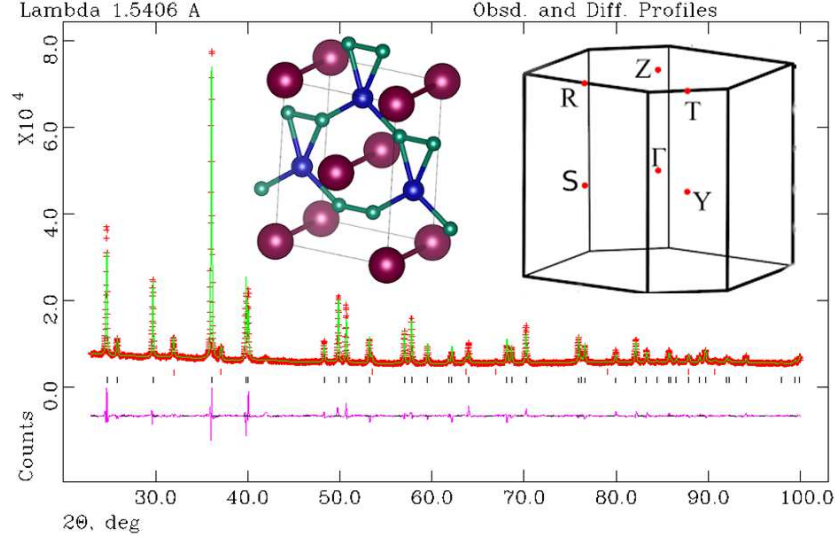


Fig. S 4: XRD pattern for YbCoC_2 at room temperature and $P = 0$ GPa (the obtained lattice parameters are listed in Table 1). The experimental points (red marks), the calculated profiles (green line) and their difference (purple line) are shown. The bars in the lower part of the graph represent the calculated Bragg reflections that correspond to the YbO impurity phase (upper row, red color) and YbCoC_2 (lower row, blue color). Inset: The unit cell (generated using the VESTA software Momma and Izumi [2011]), with the red, blue and green balls corresponding to Yb, Co and C ions (left) and the first Brillouin zone (right) of the $Amm2$ structure of YbCoC_2 .

Resistivity

The relative resistivity above $T = 40$ K could be well fitted with the model $\rho_{\text{fit}}^{-1}(T) = \rho_{\text{p}}^{-1} + \rho_{\text{B-G}}^{-1}(T)$ (see FIG. S7), where ρ_{p} - temperature-independent parallel resistivity and $\rho_{\text{B-G}}(T) = \rho_0 + A_{\text{el-ph}}T\left(\frac{T}{\Theta_{\text{D}}}\right)^4 \int_0^{\Theta_{\text{D}}/T} \frac{x^5}{(e^x - 1)(1 - e^{-x})} dx$ where ρ_0 - residual resistivity and the second term is contribution to the resistivity from electron-phonon scattering approximated by Bloch-Gruneisen

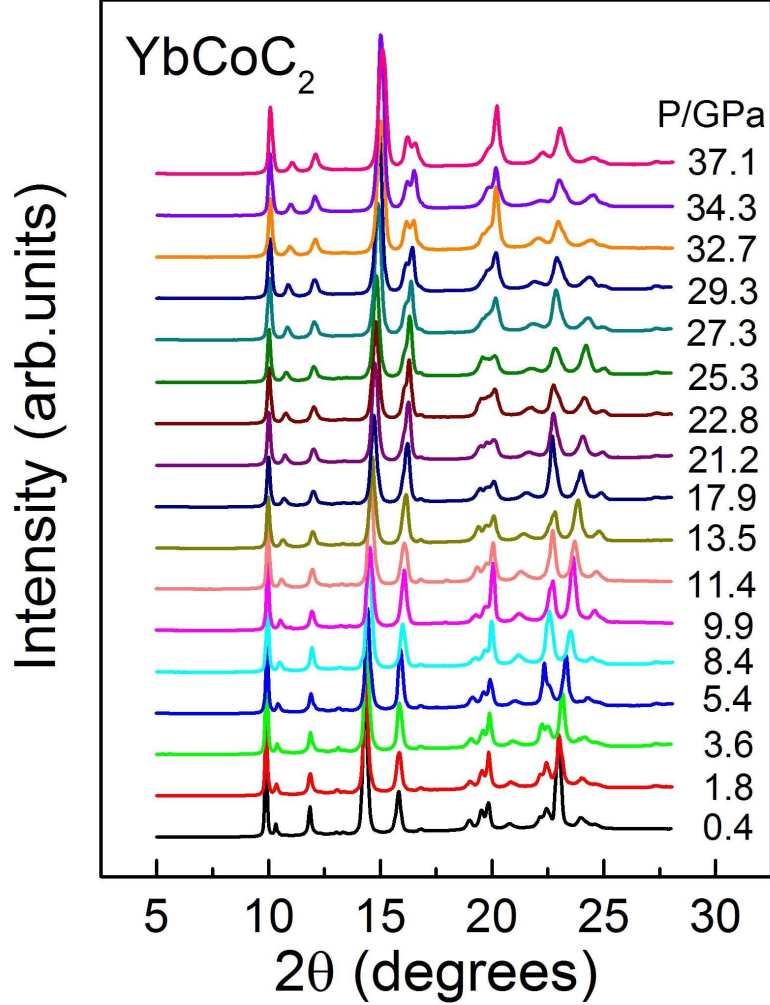


Fig. S 5: X-ray diffraction patterns of YbCoC_2 at different pressures.

law with $n = 5$ ($A_{\text{el-ph}}$ - electron-phonon coupling constant and Θ_D - Debye temperature). The best fit was obtained with the following parameters $\rho_p = 2.46(6)$, $\rho_0 = 1.62(2)$, $A_{\text{el-ph}} = 0.015(4) \text{ K}^{-1}$ and $\Theta_D = 412(3) \text{ K}$. It is interesting to note that Debye temperature determined from the resistivity is close to the average value of Debye temperature obtained from the heat capacity measurements (from heat capacity $\langle \Theta_D \rangle = \frac{m_1 \Theta_1 + m_2 \Theta_2}{m_1 + m_2} = 434(5) \text{ K}$).

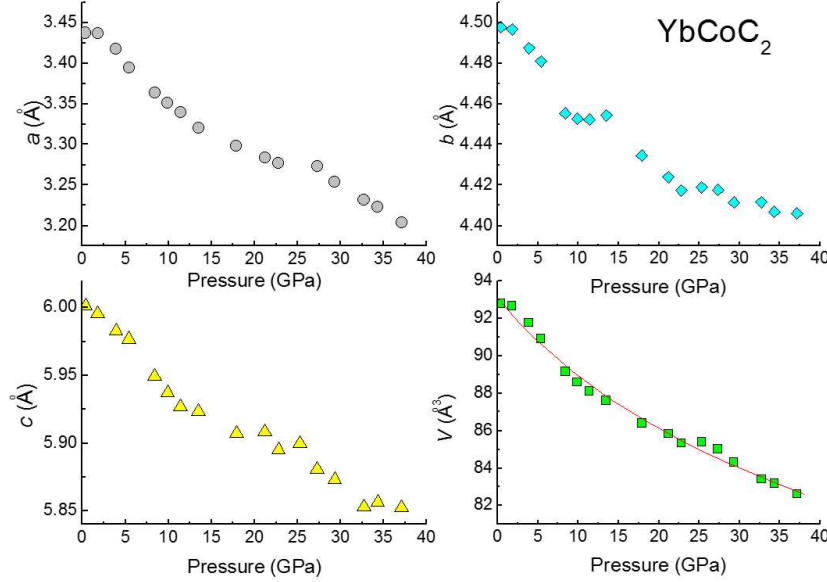


Fig. S 6: Pressure dependences of the lattice parameters and the unit cell volume of YbCoC_2 . Red line is the Murnaghan fit of experimental $V(P)$ dependence.

The careful study of the difference between measured and fitted resistivities did not reveal any anomalies above the antiferromagnetic transition temperature. The temperature derivative of the resistivity at $P = 0$ GPa near antiferromagnetic transition temperature shows a peak with a maximum at $T = 26.1(7)$ K (see inset to FIG. S7).

***Ab initio* calculations**

We employed the density-functional-theory (DFT), DFT+ U , and DFT+DMFT methods to theoretically explore electronic and magnetic properties of YbCoC_2 , with local density approximation (LDA) for exchange-correlation potential. The spin-orbit coupling (SOC) was taken into account.

Our *ab initio* DFT-LDA simulations were performed using the relativistic APW+lo method as implemented in Wien2k package Blaha et al. [2018]. For core electrons, SOC effects were included self-consistently by solving the radial Dirac equation. For valence states, the SOC was evaluated by the second-variational step MacDonald et al. [1980] using scalar-relativistic

Table 1: The crystallographic parameters of YbCoC_2 (space group $Amm2$) obtained at $T = 300$ K and $P = 0$ GPa

| X-ray diffraction $\text{Cu-K}\alpha_1$ | | | | | | | | |
|---|------------|------------|----------------|---------------|---------------|---|---|--|
| a (Å) | b (Å) | c (Å) | $z(\text{Co})$ | $y(\text{C})$ | $z(\text{C})$ | $U_{\text{iso}}(\text{Yb})$ (Å ²) | $U_{\text{iso}}(\text{Co})$ (Å ²) | $U_{\text{iso}}(\text{C})$ (Å ²) |
| 3.4391(1) | 4.4948(1) | 5.9987(1) | 0.6146(9) | 0.172(2) | 0.331(1) | 0.0176(2) | 0.0175(8) | 0.0306(34) |
| Neutron diffraction $\lambda = 2.42$ Å | | | | | | | | |
| 3.4411(9) | 4.4881(13) | 5.9925(15) | 0.643(24) | 0.154(4) | 0.311(6) | 0.0 | 0.0 | 0.0 |

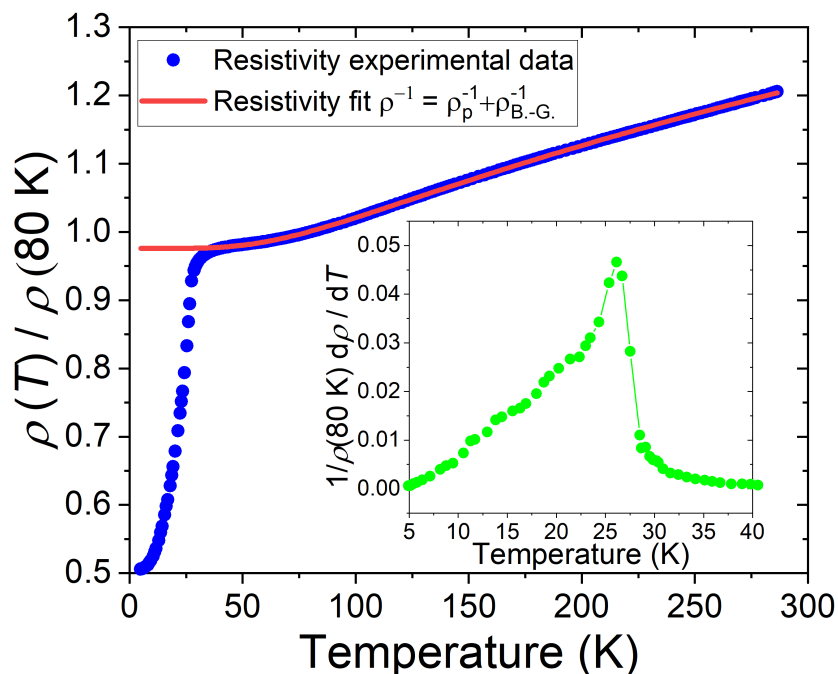


Fig. S 7: Measured resistivity relative to the value of resistivity at $T = 80$ K for YbCoC_2 at $P = 0$ GPa. The absolute value of resistivity at $T = 298$ K is $680 \mu\Omega \text{ cm}$. Blue points: experimental data, red line: fit with parallel resistor and Bloch-Gruneisen model (see text for details). Inset: the temperature derivative of resistivity at low temperatures.

eigenvectors. Since the SOC term is large only near the core, the corresponding contributions to the Hamiltonian were only evaluated inside the MT spheres surrounding the atoms. The MT-radii of Yb, Co, and C were

set to 2.50, 1.98, and 1.25 r_B , respectively. The convergence factor $R_{\min}K_{\max}$ was set to 8.0, where R_{\min} is the minimal MT-radius and K_{\max} is the plane-wave cut-off parameter, $K_{\max}^2 \approx 560$ eV. This, together with the reciprocal space resolution of $2\pi \times 0.03 \text{ \AA}^{-1}$ employed to sample the Brillouin zone (BZ) ensured the total energy convergence of about 10^{-7} eV. The calculations were made at experimental lattice periods found in this work. Starting from the experimental atomic positions, we did the geometry relaxation to allow the internal atomic coordinates to change, until the residual atomic forces were converged down to 3 meV/ \AA . The 4*f* electrons of Yb were explicitly treated as valent.

FIG. S8(a,b) presents the band structure and density of states (DOS) calculated within DFT-LDA. The DOS near Fermi energy (E_F) is mainly contributed by the hybridized 4*f*-Yb and 3*d*-Co states. The corresponding Fermi surface (FS) topology in the first BZ is shown in FIG. S8(c,d), with standard notation for the high-symmetry points. Two FS sheets related to the two spin channels of SOC are formed by the 49th and 50th bands (blue and red lines in the band structure, respectively) that cross E_F . The 3rd sheet formed by the 48th band (black line) and consisting of tiny hole-like pockets in the ΓZ direction is not shown.

In nonmagnetic YbCoC₂, a calculated value of the DOS at the Fermi level $N(E_F)$ is about of 9 st./eV = 21 mJ/(mol K²) per formula unit. As in case of other Yb-based metallic compounds, our DFT-LDA simulations (made with experimental lattice periods) demonstrate very high sensitivity of $N(E_F)$ to the choice of calculation parameters and numerical accuracy, because E_F falls at a very steep slope of the high 4*f* peak. So our estimate of $N(E_F)$ is only indicative.

We used the LDA+DMFT approach Georges et al. [1996], Kotliar et al. [2006] as implemented in the eDMFT package Haule et al. [2010]. The continuous-time quantum Monte Carlo (QMC-DMFT) impurity solver Haule [2007] was employed. The magnetic state at low temperatures was studied with the Wien2k package Blaha et al. [2018] using the LDA+*U* method Anisimov et al. [1993]. We used the rotationally invariant version Liechtenstein et al. [1995] of this method, with the parameter $U_{\text{eff}} = U - J$.

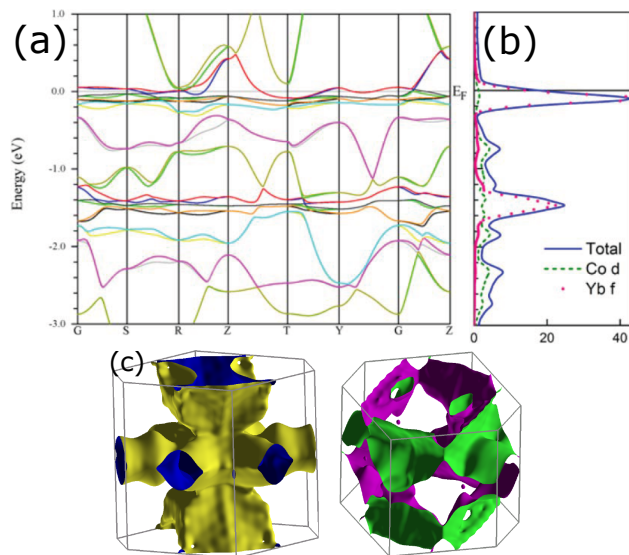


Fig. S 8: (a, b) The DFT band structure and density of states (DOS), correspondingly; the DOS is mainly contributed by hybridized $4f$ -Yb and $3d$ -Co states, other contributions are much smaller and not shown. (c, d) The Fermi surface sheets corresponding to the 49th and 50th bands, with standard notation for high-symmetry points of Brillouin zone. The FS was generated using the XCRYSDEN software Kokalj [2003].

References

See Supplemental Material below of the main text which includes Refs. Petrova et al. [2005], Mao et al. [1986], Rodriguez-Carvajal [1993], Larson and Dreele [2000], MacDonald et al. [1980], Momma and Izumi [2011], for the additional details on the experimental and computational methods.

Hidetaka Amanai, Hideya Onodera, Masayoshi Ohashi, Satoru Matsuo, Hiroshi Yamauchi, Yasuo Yamaguchi, and Noriaki Sato. Magnetic properties of the ternary carbide DyCoC_2 studied by magnetization measurements, neutron diffraction and ^{161}Dy mssbauer spectroscopy. *Journal of Magnetism and Magnetic Materials*, 148(3):413 – 418, 1995. ISSN 0304-8853. doi:[https://doi.org/10.1016/0304-8853\(95\)00024-0](https://doi.org/10.1016/0304-8853(95)00024-0). URL <http://www.sciencedirect.com/science/article/pii/0304885395000240>.

- V. I. Anisimov, I. V. Solovyev, M. A. Korotin, M. T. Czyżyk, and G. A. Sawatzky. Density-functional theory and nio photoemission spectra. *Phys. Rev. B*, 48:16929–16934, Dec 1993. doi:10.1103/PhysRevB.48.16929. URL <https://link.aps.org/doi/10.1103/PhysRevB.48.16929>.
- M.A. Avila, S.L. Budko, C. Petrovic, R.A. Ribeiro, P.C. Canfield, A.V. Tsvyashchenko, and L.N. Fomicheva. Synthesis and properties of YbB₂. *Journal of Alloys and Compounds*, 358(1):56 – 64, 2003. ISSN 0925-8388. doi:[https://doi.org/10.1016/S0925-8388\(03\)00051-3](https://doi.org/10.1016/S0925-8388(03)00051-3). URL <http://www.sciencedirect.com/science/article/pii/S0925838803000513>.
- P. Blaha, K. Schwarz, G.K.H. Madsen, D. Kvasnicka, J. Luitz, R. Laskowski, F. Tran, and L.D. Marks. *WIEN2k, An Augmented Plane Wave + Local Orbitals Program for Calculating Crystal Properties*. Karlheinz Schwarz, Techn. Universitat Wien, Austria, 2018. ISBN 3-9501031-1-2. URL <http://susi.theochem.tuwien.ac.at/index.html>.
- J. A. Blanco, D. Gignoux, and D. Schmitt. Specific heat in some gadolinium compounds. ii. theoretical model. *Phys. Rev. B*, 43:13145–13151, Jun 1991. doi:10.1103/PhysRevB.43.13145. URL <https://link.aps.org/doi/10.1103/PhysRevB.43.13145>.
- J. A. Blanco, M. de Podesta, J. I. Espeso, J. C. Gómez Sal, C. Lester, K. A. McEwen, N. Patrikios, and J. Rodríguez Fernández. Specific heat of CeNi_xPt_{1-x} pseudobinary compounds and related dilute alloys. *Phys. Rev. B*, 49:15126–15132, Jun 1994. doi:10.1103/PhysRevB.49.15126. URL <https://link.aps.org/doi/10.1103/PhysRevB.49.15126>.
- C.H. Booth, Yu Jiang, D.L. Wang, J.N. Mitchell, P.H. Tobash, E.D. Bauer, M.A. Wall, P.G. Allen, D. Sokaras, D. Nordlund, T.-C. Weng, M.A. Torrez, and J.L. Sarrao. Multiconfigurational nature of 5f orbitals in uranium and plutonium intermetallics. *Proceedings of the National Academy of Sciences*, 109(26):10205–10209, 2012. ISSN 0027-8424. doi:10.1073/pnas.1200725109. URL <https://www.pnas.org/content/109/26/10205>.
- S. Chattopadhyay, V. Simonet, V. Skumryev, A. A. Mukhin, V. Yu. Ivanov, M. I. Aroyo, D. Z. Dimitrov, M. Gospodinov, and E. Ressouche. Single-crystal neutron diffraction study of hexagonal multiferroic YbMnO₃ under a magnetic field. *Phys. Rev. B*, 98:134413, Oct 2018.

- doi:10.1103/PhysRevB.98.134413. URL <https://link.aps.org/doi/10.1103/PhysRevB.98.134413>.
- S. Danzenbächer, D. V. Vyalikh, K. Kummer, C. Krellner, M. Holder, M. Höppner, Yu. Kucherenko, C. Geibel, M. Shi, L. Patthey, S. L. Molodtsov, and C. Laubschat. Insight into the f -derived fermi surface of the heavy-fermion compound YbRh_2Si_2 . *Phys. Rev. Lett.*, 107:267601, Dec 2011. doi:10.1103/PhysRevLett.107.267601. URL <https://link.aps.org/doi/10.1103/PhysRevLett.107.267601>.
- De Gennes, P.G. Polarisation de charge (ou de spin) au voisinage d'une impureté dans un alliage. *J. Phys. Radium*, 23(10):630–636, 1962. doi:10.1051/jphysrad:019620023010063000. URL <https://doi.org/10.1051/jphysrad:019620023010063000>.
- S. Doniach. The kondo lattice and weak antiferromagnetism. *Physica B+C*, 91:231 – 234, 1977. ISSN 0378-4363. doi:[https://doi.org/10.1016/0378-4363\(77\)90190-5](https://doi.org/10.1016/0378-4363(77)90190-5). URL <http://www.sciencedirect.com/science/article/pii/0378436377901905>.
- Takao Ebihara, Yoshihiko Inada, Masao Murakawa, Shinya Uji, Chieko Terakura, Taichi Terashima, Etsuji Yamamoto, Yoshinori Haga, Yoshichika nuki, and Hisatomo Harima. Heavy fermions in YbAl_3 studied by the de haas-van alphen effect. *Journal of the Physical Society of Japan*, 69(3):895–899, 2000. doi:10.1143/JPSJ.69.895. URL <https://doi.org/10.1143/JPSJ.69.895>.
- Kentaro Enoki, Yusuke Hirose, Shingo Yoshiuchi, Kiyohiro Sugiyama, Fuminori Honda, Tetsuya Takeuchi, Etsuji Yamamoto, Yoshinori Haga, Masayuki Hagiwara, Koichi Kindo, Rikio Settai, and Yoshichika nuki. Electronic and magnetic properties in heavy fermion ferromagnet YbPdGe . *Journal of the Physical Society of Japan*, 81(Suppl.B):SB056, 2012. doi:10.1143/JPSJS.81SB.SB056. URL <https://doi.org/10.1143/JPSJS.81SB.SB056>.
- Z. Fisk, P. C. Canfield, W. P. Beyermann, J. D. Thompson, M. F. Hundley, H. R. Ott, E. Felder, M. B. Maple, M. A. Lopez de la Torre, P. Visani, and C. L. Seaman. Massive electron state in YbBiPt . *Phys. Rev. Lett.*, 67:3310–3313, Dec 1991. doi:10.1103/PhysRevLett.67.3310. URL <https://link.aps.org/doi/10.1103/PhysRevLett.67.3310>.

- P. Gegenwart, J. Custers, C. Geibel, K. Neumaier, T. Tayama, K. Tenya, O. Trovarelli, and F. Steglich. Magnetic-field induced quantum critical point in YbRh_2Si_2 . *Phys. Rev. Lett.*, 89:056402, Jul 2002. doi:10.1103/PhysRevLett.89.056402. URL <https://link.aps.org/doi/10.1103/PhysRevLett.89.056402>.
- Antoine Georges, Gabriel Kotliar, Werner Krauth, and Marcelo J. Rozenberg. Dynamical mean-field theory of strongly correlated fermion systems and the limit of infinite dimensions. *Rev. Mod. Phys.*, 68:13–125, Jan 1996. doi:10.1103/RevModPhys.68.13. URL <https://link.aps.org/doi/10.1103/RevModPhys.68.13>.
- F. Haslbeck, S. Säubert, M. Seifert, C. Franz, M. Schulz, A. Heinemann, T. Keller, Pinaki Das, J. D. Thompson, E. D. Bauer, C. Pfleiderer, and M. Janoschek. Ultrahigh-resolution neutron spectroscopy of low-energy spin dynamics in UGe_2 . *Phys. Rev. B*, 99:014429, Jan 2019. doi:10.1103/PhysRevB.99.014429. URL <https://link.aps.org/doi/10.1103/PhysRevB.99.014429>.
- Kristjan Haule. Quantum monte carlo impurity solver for cluster dynamical mean-field theory and electronic structure calculations with adjustable cluster base. *Phys. Rev. B*, 75:155113, Apr 2007. doi:10.1103/PhysRevB.75.155113. URL <https://link.aps.org/doi/10.1103/PhysRevB.75.155113>.
- Kristjan Haule, Chuck-Hou Yee, and Kyoo Kim. Dynamical mean-field theory within the full-potential methods: Electronic structure of CeIrIn_5 , CeCoIn_5 , and CeRhIn_5 . *Phys. Rev. B*, 81:195107, May 2010. doi:10.1103/PhysRevB.81.195107. URL <https://link.aps.org/doi/10.1103/PhysRevB.81.195107>.
- W. Jeitschko and M.H. Gerss. Ternary carbides of the rare earth and iron group metals with CeCoC_2 - and CeNiC_2 -type structure. *Journal of the Less Common Metals*, 116(1):147 – 157, 1986. ISSN 0022-5088. doi:[https://doi.org/10.1016/0022-5088\(86\)90225-0](https://doi.org/10.1016/0022-5088(86)90225-0). URL <http://www.sciencedirect.com/science/article/pii/0022508886902250>.
- Mitsuo Kasaya, Hiroyuki Suzuki, Takeshi Yamaguchi, and Kenichi Katoh. Magnetic properties of new ternary rare earth compounds $\text{rpt}(\text{pd})\text{sb}$. *Journal of the Physical Society of Japan*, 61(11):4187–4192, 1992.

doi:10.1143/JPSJ.61.4187. URL <https://doi.org/10.1143/JPSJ.61.4187>.

Susumu Katano, Kohei Shibata, Kotaro Nakashima, Hideaki Yoshimura, and Yohei Matsubara. Competition between superconductivity and magnetism in non-centrosymmetric $\text{La}_{1-x}\text{Ce}_x\text{NiC}_2$. *Journal of the Physical Society of Japan*, 86(10):104704, 2017. doi:10.7566/JPSJ.86.104704. URL <https://doi.org/10.7566/JPSJ.86.104704>.

Kenichi Katoh, Seisuke Nakagawa, Giichi Terui, and Akira Ochiai. Magnetic and transport properties of single-crystal YbPtGe. *Journal of the Physical Society of Japan*, 78(10):104721, 2009. doi:10.1143/JPSJ.78.104721. URL <https://doi.org/10.1143/JPSJ.78.104721>.

Anton Kokalj. Computer graphics and graphical user interfaces as tools in simulations of matter at the atomic scale. *Computational Materials Science*, 28(2):155 – 168, 2003. ISSN 0927-0256. doi:[https://doi.org/10.1016/S0927-0256\(03\)00104-6](https://doi.org/10.1016/S0927-0256(03)00104-6). URL <http://www.sciencedirect.com/science/article/pii/S0927025603001046>.

G. Kotliar, S. Y. Savrasov, K. Haule, V. S. Oudovenko, O. Parcollet, and C. A. Marianetti. Electronic structure calculations with dynamical mean-field theory. *Rev. Mod. Phys.*, 78:865–951, Aug 2006. doi:10.1103/RevModPhys.78.865. URL <https://link.aps.org/doi/10.1103/RevModPhys.78.865>.

A.C. Larson and R.B. Von Dreele. General structure analysis system (gsas). *Los Alamos National Laboratory Report LAUR*, 86-748, 2000. URL http://www.nist.gov/cgi-bin/exit_nist.cgi?url=http://www.ccp14.ac.uk/ccp/ccp14/ftp-mirror/gsas/public/gsas/manual/GSASManual.pdf.

A. I. Liechtenstein, V. I. Anisimov, and J. Zaanen. Density-functional theory and strong interactions: Orbital ordering in mott-hubbard insulators. *Phys. Rev. B*, 52:R5467–R5470, Aug 1995. doi:10.1103/PhysRevB.52.R5467. URL <https://link.aps.org/doi/10.1103/PhysRevB.52.R5467>.

A H MacDonald, W E Pickett, and D D Koelling. A linearised relativistic augmented-plane-wave method utilising approximate pure spin basis

- functions. *Journal of Physics C: Solid State Physics*, 13(14):2675–2683, may 1980. doi:10.1088/0022-3719/13/14/009. URL <https://doi.org/10.1088%2F0022-3719%2F13%2F14%2F009>.
- H. K. Mao, J. Xu, and P. M. Bell. Calibration of the ruby pressure gauge to 800 kbar under quasi-hydrostatic conditions. *Journal of Geophysical Research: Solid Earth*, 91(B5):4673–4676, 1986. doi:10.1029/JB091iB05p04673. URL <https://agupubs.onlinelibrary.wiley.com/doi/abs/10.1029/JB091iB05p04673>.
- Koichi Momma and Fujio Izumi. *VESTA3* for three-dimensional visualization of crystal, volumetric and morphology data. *Journal of Applied Crystallography*, 44(6):1272–1276, Dec 2011. doi:10.1107/S0021889811038970. URL <https://doi.org/10.1107/S0021889811038970>.
- Kiyochiro Motoya, Keisuke Nakaguchi, Noriaki Kayama, Kazunori Inari, Jun Akimitsu, Koichi Izawa, and Toshizo Fujita. Magnetic properties of CeNiC₂ structure by macroscopic and microscopic measurements. *Journal of the Physical Society of Japan*, 66(4):1124–1129, 1997. doi:10.1143/JPSJ.66.1124.
- H.R. Ott, H. Rudigier, and F. Hulliger. Low-temperature phase transitions in Yb monpnictides. *Solid State Communications*, 55(2): 113 – 116, 1985. ISSN 0038-1098. doi:[https://doi.org/10.1016/0038-1098\(85\)90259-5](https://doi.org/10.1016/0038-1098(85)90259-5). URL <http://www.sciencedirect.com/science/article/pii/0038109885902595>.
- Alla E. Petrova, Vladimir A. Sidorov, and Sergei M. Stishov. High-pressure helium gas apparatus and hydrostatic toroid cell for low-temperatures applications. *Physica B: Condensed Matter*, 359-361:1463 – 1465, 2005. ISSN 0921-4526. doi:<https://doi.org/10.1016/j.physb.2005.01.454>. URL <http://www.sciencedirect.com/science/article/pii/S0921452605004850>.
- B. Pollit, D. Drkop, and P. Weidner. Magnetic ordering of mixed valent Yb₃Pd₄. *Journal of Magnetism and Magnetic Materials*, 47-48: 583 – 585, 1985. ISSN 0304-8853. doi:[https://doi.org/10.1016/0304-8853\(85\)90501-3](https://doi.org/10.1016/0304-8853(85)90501-3). URL <http://www.sciencedirect.com/science/article/pii/0304885385905013>.

- R. Pott, W. Boksich, G. Leson, B. Politt, H. Schmidt, A. Freimuth, K. Keulerz, J. Langen, G. Neumann, F. Oster, J. Röhler, U. Walter, P. Weidner, and D. Wohlleben. Magnetic order and other phase transitions in mixed-valent YbPd. *Phys. Rev. Lett.*, 54:481–484, Feb 1985. doi:10.1103/PhysRevLett.54.481. URL <https://link.aps.org/doi/10.1103/PhysRevLett.54.481>.
- Juan Rodriguez-Carvajal. Recent advances in magnetic structure determination by neutron powder diffraction. *Physica B: Condensed Matter*, 192(1):55 – 69, 1993. ISSN 0921-4526. doi:[https://doi.org/10.1016/0921-4526\(93\)90108-I](https://doi.org/10.1016/0921-4526(93)90108-I). URL <http://www.sciencedirect.com/science/article/pii/092145269390108I>.
- D. P. Rojas, L. Fernández Barquín, C. Echevarria-Bonet, and J. Rodríguez Fernández. YbNi₂: A heavy fermion ferromagnet. *Solid State Communications*, 152:1834–1837, October 2012. doi:10.1016/j.ssc.2012.07.001.
- C. Rossel, K. N. Yang, M. B. Maple, Z. Fisk, E. Zirngiebl, and J. D. Thompson. Strong electronic correlations in a new class of Yb-based compounds: YbXCu₄ (X = Ag,Au,Pd). *Phys. Rev. B*, 35:1914–1918, Feb 1987. doi:10.1103/PhysRevB.35.1914. URL <https://link.aps.org/doi/10.1103/PhysRevB.35.1914>.
- W. Schfer, G. Will, P.A. Kotsanidis, and J.K. Yakinthos. Magnetic properties of RCoC₂ (R = Y, Gd, Tb) compounds. *Journal of Magnetism and Magnetic Materials*, 88(1):13 – 17, 1990. ISSN 0304-8853. doi:[https://doi.org/10.1016/S0304-8853\(97\)90005-6](https://doi.org/10.1016/S0304-8853(97)90005-6). URL <http://www.sciencedirect.com/science/article/pii/S0304885397900056>.
- W Schfer, W Kockelmann, G Will, J.K Yakinthos, and P.A Kotsanidis. Magnetic structures of rare earths R in RCoC₂ and RNiC₂ compounds. *Journal of Alloys and Compounds*, 250(1):565 – 568, 1997. ISSN 0925-8388. doi:[https://doi.org/10.1016/S0925-8388\(96\)02564-9](https://doi.org/10.1016/S0925-8388(96)02564-9). URL <http://www.sciencedirect.com/science/article/pii/S0925838896025649>.
- Shintaro Suzuki, Kou Takubo, Kentaro Kuga, Wataru Higemoto, Takashi U. Ito, Takahiro Tomita, Yasuyuki Shimura, Yosuke Matsumoto, Cedric Bareille, Hiroki Wadati, Shik Shin, and Satoru Nakatsuji, 2018.

- Takashi Takahashi, Noriaki Sato, Takayoshi Yokoya, Ashish Chainani, Takayuki Morimoto, and Takemi Komatsubara. Dual character of 5f electrons in UPd₂Al₃ observed by high-resolution photoemission spectroscopy. *Journal of the Physical Society of Japan*, 65(1):156–159, 1996. doi:10.1143/JPSJ.65.156. URL <https://doi.org/10.1143/JPSJ.65.156>.
- Takahiro Tomita, Kentaro Kuga, Yoshiya Uwatoko, Piers Coleman, and Satoru Nakatsuji. Strange metal without magnetic criticality. *Science*, 349(6247):506–509, 2015. ISSN 0036-8075. doi:10.1126/science.1262054. URL <https://science.sciencemag.org/content/349/6247/506>.
- Takahiro Tomita, Kentaro Kuga, Yoshiya Uwatoko, and Satoru Nakatsuji. Pressure-induced magnetic transition exceeding 30 K in the Yb-based heavy-fermion β -YbAlB₄. *Phys. Rev. B*, 94:245130, Dec 2016. doi:10.1103/PhysRevB.94.245130. URL <https://link.aps.org/doi/10.1103/PhysRevB.94.245130>.
- R. Troć, Z. Gajek, and A. Pikul. Dualism of the 5f electrons of the ferromagnetic superconductor UGe₂ as seen in magnetic, transport, and specific-heat data. *Phys. Rev. B*, 86:224403, Dec 2012. doi:10.1103/PhysRevB.86.224403. URL <https://link.aps.org/doi/10.1103/PhysRevB.86.224403>.
- Naohito Tsujii, Kenichi Katoh, Lukas Keller, Andreas Dnni, Noriki Terada, and Hideaki Kitazawa. Magnetic structure of the ferromagnetic kondo-lattice compounds YbPtGe and YbPdGe. *Journal of Physics: Condensed Matter*, 27(32):325601, jul 2015. doi:10.1088/0953-8984/27/32/325601. URL <https://doi.org/10.1088/0953-8984/27/32/325601>.
- A.V. Tsvyashchenko. High pressure synthesis of RE₆Cu₂₃ compounds (RE = Tb, Dy, Yb, Lu). *Journal of the Less Common Metals*, 99(2):L9 – L11, 1984. ISSN 0022-5088. doi:[https://doi.org/10.1016/0022-5088\(84\)90231-5](https://doi.org/10.1016/0022-5088(84)90231-5). URL <http://www.sciencedirect.com/science/article/pii/0022508884902315>.
- B. G. Ueland, A. Kreyssig, K. Prokeš, J. W. Lynn, L. W. Harriger, D. K. Pratt, D. K. Singh, T. W. Heitmann, S. Sauerbrei, S. M. Saunders, E. D. Mun, S. L. Bud'ko, R. J. McQueeney, P. C. Canfield, and A. I. Goldman. Fragile antiferromagnetism in the heavy-fermion compound YbBiPt. *Phys.*

Rev. B, 89:180403(R), May 2014. doi:10.1103/PhysRevB.89.180403. URL <https://link.aps.org/doi/10.1103/PhysRevB.89.180403>.

U. Walter, Z. Fisk, and E. Holland-Moritz. Magnetic excitations and quasielastic linewidths in YbBe_{13} from neutron scattering. *Journal of Magnetism and Magnetic Materials*, 47-48:159 – 162, 1985. ISSN 0304-8853. doi:[https://doi.org/10.1016/0304-8853\(85\)90386-5](https://doi.org/10.1016/0304-8853(85)90386-5). URL <http://www.sciencedirect.com/science/article/pii/0304885385903865>.

J.O. Willis, J.L. Smith, and Z. Fisk. Unusual magnetic behavior of TmIr_2 and YbIr_2 . *Journal of Magnetism and Magnetic Materials*, 47-48:581 – 582, 1985. ISSN 0304-8853. doi:[https://doi.org/10.1016/0304-8853\(85\)90500-1](https://doi.org/10.1016/0304-8853(85)90500-1). URL <http://www.sciencedirect.com/science/article/pii/0304885385905001>.

A. Yaouanc, P. Dalmas de Réotier, P. C. M. Gubbens, C. T. Kaiser, A. A. Menovsky, M. Mihalik, and S. P. Cottrell. Evidence for weak itinerant long-range magnetic correlations in UGe_2 . *Phys. Rev. Lett.*, 89:147001, Sep 2002. doi:10.1103/PhysRevLett.89.147001. URL <https://link.aps.org/doi/10.1103/PhysRevLett.89.147001>.

A Yaouanc, P Dalmas de Réotier, L Keller, B Roessli, and A Forget. A novel type of splayed ferromagnetic order observed in $\text{Yb}_2\text{Ti}_2\text{O}_7$. *Journal of Physics: Condensed Matter*, 28(42):426002, aug 2016. doi:10.1088/0953-8984/28/42/426002. URL <https://doi.org/10.1088/0953-8984/28/42/426002>.

G Zwicknagl and P Fulde. The dual nature of $5f$ electrons and the origin of heavy fermions in U compounds. *Journal of Physics: Condensed Matter*, 15(28):S1911–S1916, jul 2003. doi:10.1088/0953-8984/15/28/302. URL <https://doi.org/10.1088/0953-8984/15/28/302>.